Anomalous Sensor Response of TiO2 Films: Electrochemical Impedance Spectroscopy and ab Initio Studies

ARTICLE *in* THE JOURNAL OF PHYSICAL CHEMISTRY C · DECEMBER 2009

Impact Factor: 4.77 · DOI: 10.1021/jp9024014

CITATIONS
10

READS
41

3 AUTHORS:

Marciano Sánchez
University of Guadalajara
10 PUBLICATIONS **190** CITATIONS
SEE PROFILE

Marina Rincón
Universidad Nacional Autónoma de México
94 PUBLICATIONS **1,326** CITATIONS
SEE PROFILE

R. A. Guirado-Lopez
Universidad Autónoma de San Luis Potosí
57 PUBLICATIONS **687** CITATIONS
SEE PROFILE

Anomalous Sensor Response of TiO_2 Films: Electrochemical Impedance Spectroscopy and ab Initio Studies

Marciano Sánchez, Marina E. Rincón,* and Ricardo A. Guirado-López

Centro de Investigación en Energía, Universidad Nacional Autónoma de México, Apartado Postal 34, Temixco 62580, MOR, México; RAGL Instituto de Física "Manuel Sandoval Vallarta", UASLP, Álvaro Obregón 64, San Luis Potosí, 78000, SLP, México

Received: March 17, 2009; Revised Manuscript Received: November 11, 2009

In this paper, we report the elaboration of TiO_2 thin films ($\sim$0.25 μm) from sol−gel solutions by dip-coating and annealing techniques as well as the annealing temperature-dependent response of these films when sensing ammonia. Electrochemical impedance spectroscopy studies revealed that films annealed at 400 °C show an anomalous p-type behavior manifested by an increase in resistance and capacitance upon ammonia adsorption, an electron donor molecule, while a typical n-type behavior is found in films annealed at 600 °C where the decrease in resistance is in accord with the ammonia present. To understand the possible physical origin of the measured data, we perform ab initio pseudopotential density functional theory (DFT) calculations to analyze the energetics, structural properties, and electronic behavior of NH_3 molecules adsorbed on small-model Ti_xO_y ($x = 4$, $y = 6-8$) clusters. We also use the nudged elastic band (NEB) method to analyze possible reaction pathways and transition states that could be present in the here-considered $Ti_xO_y + NH_3$ systems. We found that dissociative NH_3 adsorption leads to a reversed $Ti_xO_y \rightarrow$ adsorbate direction for the charge transfer, which is a fact that is expected to increase the resistance in electron-conducting systems, as observed in our TiO_2 samples annealed at 400 °C. The energy barriers that need to be overcome to achieve the here-predicted dissociation reaction strongly depend on the local atomic environment around the adsorption site being particularly reduced when poorly coordinated Ti sites are present in the clusters.

Introduction

Titanium dioxide is a metallic oxide with several environmental and energy related applications such as heterogeneous catalysis, gas sensors, and solar cells. As a sensor, TiO_2 has been used to monitor organic vapors[1,2] as well as oxidant and reducing gases.[3−6] Major problems with TiO_2 are its cross-sensitivity and high resistivity (10^6 Ω cm) that require high temperatures (300−500 °C) for sensing. Some novel strategies to overcome these problems are the use of high surface area nanometric TiO_2 and the introduction of transition metals to induce selectivity and to avoid grain growth.[7−10]

Mixed rutile/anatase phases have proved to be beneficial in photocatalytic application, but in previous work, we found little influence of the various crystalline phases of TiO_2 (i.e., mixed or pure phases) on ammonia sensing with the coordination environment around the surface Ti sites being more important.[11,12] TiO_2 usually shows n-type behavior (i.e., electron conductivity) manifested by a decrease in resistance when exposed to electron donor reducing gases and by an increase in resistance upon adsorption of electron-withdrawing oxidants. This well-known sensitivity has made the resistor-sensing platform the preferred one. Resistor-like sensors respond to the changes on bulk properties (Fermi level) caused by the adsorbed molecules, while Schottky sensors respond to the modulation of the film/electrode junction properties, and sensors based on thin films transistors usually show a combination of both mechanisms.[13]

To study the details of the adsorbant−adsorbate interaction, not many works report the use of spectroscopy techniques to discriminate among the various physicochemical events taking place.[14−16] In the present contribution, the changes in impedance of TiO_2 films upon ammonia adsorption were followed by electrochemical impedance spectroscopy (EIS), and surprisingly, the film's conductivity shows a dependence on the film's annealing temperature, which was not observed in the resistor platform. Our experimental studies reveal that TiO_2 films annealed at 400 °C show an anomalous p-type behavior manifested by an increase in resistance and capacitance upon ammonia adsorption, while typical n-type behavior is found in films annealed at 600 °C where the decrease in resistance is in accord with the ammonia present.

To shed some light, at a molecular level, into the physical origin of the here-reported anomalous transport properties, the experimental results will be compared with ab initio pseudopotential density functional theory (DFT) calculations addressing the NH_3 adsorption on small Ti_xO_y ($x = 4$, $y = 6-8$) clusters. Even if the theoretical results will not be strictly comparable with the ones found in the synthesized TiO_2 surfaces, we hope that these model systems will capture the main physics of ammonia molecules adsorbed on complex titanium dioxide nanostructures.

The most important issue that needs to be addressed is if there are some well-defined details of the local geometrical and chemical environment that could be at the origin of the anomalous measured data. As is well-known, direct experimental determination of the surface structure remains extremely challenging and, as a consequence, we will analyze the adsorption of the NH_3 molecule on various Ti_xO_y clusters with different sizes and chemical compositions. In addition, we will study also some surface reactions that could lead to dissociated molecular configurations. We will thus determine the atomic structure of adsorbed ammonia in various precursors (NH_3) and dissociated

* To whom correspondence should be addressed. Tel: +52-55-56229752. Fax: +52-55-56229742. E-mail: merg@cie.unam.mx.

10.1021/jp9024014
Published on Web 12/07/2009

(NH_2 + H) states. The reaction pathways as well as the barriers for the elementary steps will be obtained by using the nudged elastic band (NEB) method,[17] which is an efficient technique for finding the minimum energy path between reactants and products. The relatively small size of our model cluster systems will ensure that the calculations for the reaction pathways will remain computationally tractable. In all cases, we will analyze the magnitude and direction of the charge transfer between the interacting species by performing a Lowdin population analysis.[18]

Experimental Section

TiO_2 Film Elaboration and Characterization. TiO_2 thin films were elaborated by dip-coating/annealing cycles using a sol−gel solution containing 0.025 mL HCl (JT-Baker), 8 mL titanium isopropoxide (Sigma-Aldrich), and 92 mL 2-propanol (Sigma-Aldrich). The solution (pH = 6) was aged for 2 days at room temperature (27 °C). Films were deposited on ITO substrates (indium tin oxide, Delta Technologies Limited, R_s = 13−15 Ω) at 40 mm/min dipping and withdrawing speed. Drying was carried out at 400 °C in air for 5 min. After 15 immersions, the films were annealed in air for 1 h at either 400 or 600 °C.

Film crystallinity was determined by X-ray diffraction studies (Rigaku Dmax 2200 diffractometer with Cu Kα radiation) using the Bragg−Brentano configuration in the 2θ range from 10° to 70°. Chemical composition analysis was carried out with Jade-Midi software, and the determination of crystallite size was carried out by the Debye−Scherrer equation.[19] Film surface topography and phase images were obtained by atomic force microscopy (AFM) using a Nanosurf Easyscan 2 AFM unit (Nanosurf AG, Switzerland) in tapping mode combined with contrast phase mode at 200−300 mV free amplitude and 50−80% set point. Image digital processing was done with Gwyddion GNU General Public License software (Czech Metrology Institute). Film thickness was measured with an Alpha Step perfilometer (Tencor Instruments) before impedance measurements were carried out with a Solartron SI 1267 potentiostat working with a Solartron SI 1260 frequency response analyzer. Impedance data were analyzed with Zview (Scribner Associates Inc.) and Zsimpwin (Princeton Applied Research) software fitting the experimental curves by complex nonlinear least-squares (CNLS) method to obtain the best equivalent circuits. A two-electrode sandwich cell consisting of an ITO substrate−TiO_2 film (working electrode) and a silver electrode painted onto the TiO_2 surface (counter electrode) was used for impedance measurements carried out in the frequency range from 10 mHz to 10^7 Hz. The two-electrode configuration was introduced in a closed vessel, where the first measurement was performed under air, the second measurement was taken 5 min after introducing 1 vol % NH_3 concentration in 150 mL/min nitrogen flow, and the subsequent readings corresponded to 4 vol % NH_3 taken with 5 min intervals.

Theoretical Calculations. The energetics, structural properties, and electronic behavior of NH_3 molecules adsorbed on small Ti_xO_y ($x = 4$, $y = 6-8$) clusters, as well as the minimum energy paths between reactants and products, were obtained within the DFT approach using the ultrasoft pseudopotential approximation for the electron−ion interaction and a plane-wave basis set for the wave functions as implemented in the PWscf code.[20] In all our structural optimization calculations, the cutoff energy for the plane-wave expansion was 340 eV. Values larger than the previous one have been found to lead to very small variations in the interatomic distances and bonding angles of the here-considered NH_3 + titanium dioxide nanostructures A cubic supercell with a side dimension of 25 Å was employed in the calculations, which assures a negligible interaction between the images in our supercell approach and the gamma point for the Brillouin zone integration. In all cases, we used the Perdew−Wang gradient-corrected functional,[21] and we performed both constrained and fully unconstrained structural optimizations using the conjugate gradient method. The convergence in energy was set as 1 meV, and the structural optimization was performed until a value of less than 1 meV/Å was achieved for the remaining forces for each atom.

To determine the minimum energy paths (in a static approximation) as well as the transient states, we applied the NEB method.[17] The NEB method is a chain-of-states method where a set of images between the initial and final states must be created to achieve a smooth curve. In all our calculations, we have always used at least seven images to determine the energy profile, which have been found to be enough to clearly reveal the different stages of the partial dissociation reaction of the adsorbed NH_3 group on the Ti_xO_y clusters. The determination of the minimum energy paths was found to be in some cases more sensitive to the cutoff energy value of the plane-wave expansion. Consequently, for this type of calculation, the cutoff was increased to 408 eV in order to obtain in general negligible variations in the shape of the energy profiles. Finally, the relevant energy barriers between well-defined reactants and products were obtained by calculating the energy difference of the initial position and the saddle point of each one of the energy profiles.

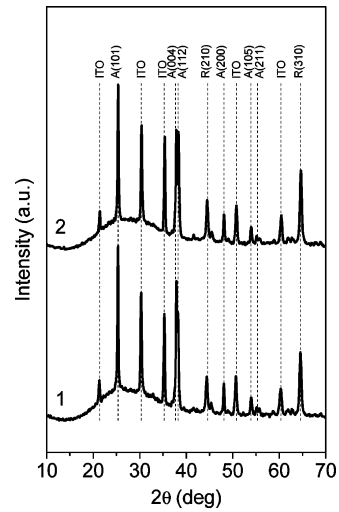

Figure 1. XRD patterns of dip-coated TiO_2 thin films annealed in air for 1 h at 400 °C (1) and 600 °C (2). ITO, indium tin oxide; A, anatase; R, rutile.

Results

XRD, AFM, and EIS. Figure 1 presents the XRD pattern of dip-coating TiO_2 thin films (∼250 nm thickness) annealed at 400 and 600 °C. Two phases are evident (anatase and rutile) as well as the preferential growth of the (101) crystalline planes in anatase and the (310) crystalline planes in rutile. The incipient transformation of anatase into rutile can be inferred from the minor enrichment of the rutile phase at 600 °C. For both annealing temperatures, the calculated crystallite size computed by the Debye−Scherrer equation was in the range of 30−35 nm for anatase and was 20 nm for rutile, but from AFM measurements (Figure 2), it is clear that at 600 °C there is an

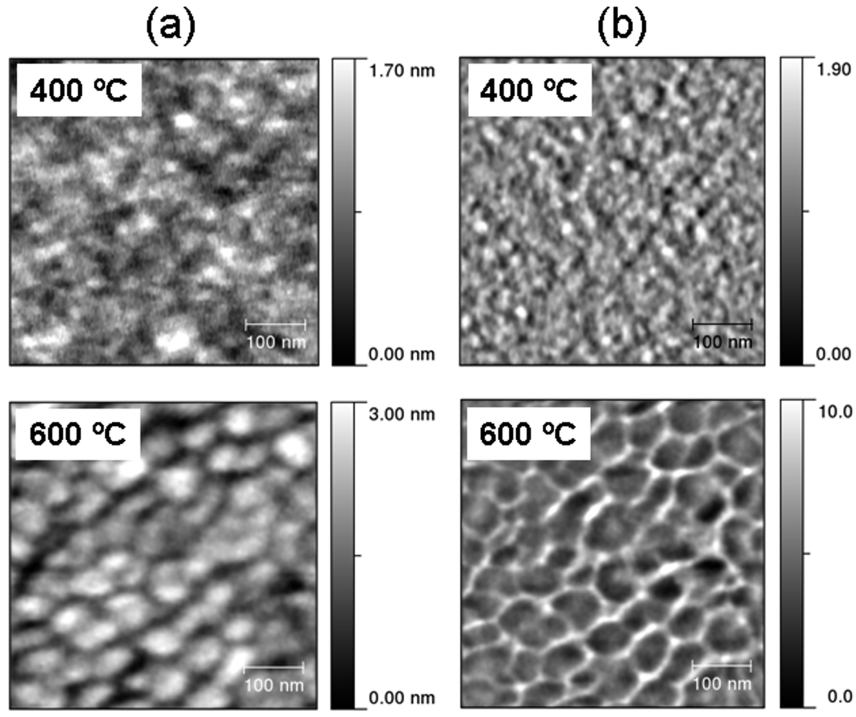

Figure 2. AFM images of dip-coated TiO_2 thin films annealed in air for 1 h at 400 and 600 °C. (a) Film topography. (b) Phase diagrams.

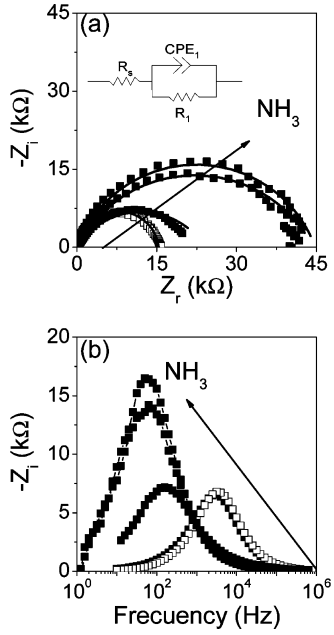

Figure 3. Electrochemical impedance spectroscopy of TiO_2 thin films air-annealed at 400 °C and exposed to air (empty squares) and to a range of ammonia concentrations (solid squares): (a) Nyquist plot and equivalent circuit; (b) imaginary impedance vs frequency plots. The arrow indicates the direction of increasing ammonia concentration. Experimental curve (squares), fitted curve (continuous line).

enlargement in particle size caused by a higher degree of sintering (i.e., for films annealed at 600 °C, the mean grain size was 44 nm vs the 26 nm value obtained for films annealed at 400 °C).

Figure 3 shows the electrochemical impedance spectroscopy results of TiO_2 films annealed a 400 °C. Here, as the ammonia concentration or exposure time increases, the overall impedance of the two-electrode cell increases in contrast with the decrease observed in the resistor platform (results not shown). Fitting the EIS curves with an equivalent circuit consisting of a resistor

TABLE 1: Values of Equivalent Circuit Elements Used To Fit the EIS Data during Ammonia Adsorption on TiO_2 Thin Films Annealed at 400 °C and Relaxation Times and Sensitivity Values

	air	NH_3 1%	NH_3 4% 5 min	NH_3 4% 10 min	NH_3 4% 15 min
R_s (Ω)	16	19	22	43	61
R_1 (kΩ)	15	15	24	44	45
Q_1^0 (nSs^{n1})	5	7	550	390	230
n_1	0.95	0.93	0.65	0.70	0.78
C_1 (nF)	3.1	3.3	54	69	64
τ_1 (ms)	0.05	0.05	1.3	3.0	2.9
S (%)		0.1	56	188	190

R_s in series with a Randle loop [i.e., a constant phase element (Q_1) in parallel to a resistor R_1] let us quantify the evolution of these circuit elements with respect to ammonia exposure. Q usually refers to an imperfect capacitor and its impedance is given by the relation[22]

$$Z_{CPE} = \frac{1}{Q^0(j\omega)^n} \tag{1}$$

where ω is the angular frequency and n varies between 0.5 and 1. True capacitance values were computed from the relation[23]

$$C = \frac{(Q^0 \times R)^{(1/n)}}{R} \tag{2}$$

Relaxation times (τ) and sensitivities (S) were calculated using the following relations:

$$\tau = RC \tag{3}$$

$$S = \frac{[(R_s + R_1)_{ammonia} - (R_s + R_1)_{air}]}{(R_s + R_1)_{air}} \times 100 \tag{4}$$

From Table 1, we can see that all the important variables (C_1, τ_1, S, and R_1) increase as time and ammonia concentration do. R_s (circuit element in the order of Ω) has been related to the sum of wire resistance and titania's bulk resistance, while

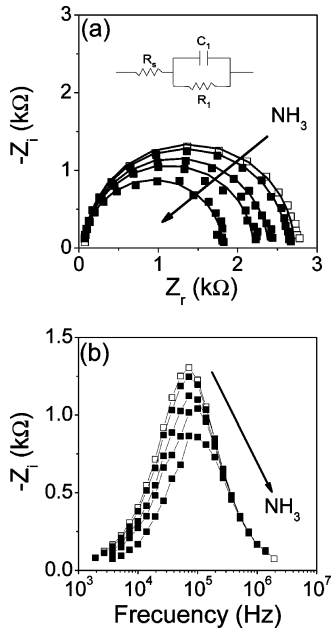

Figure 4. Electrochemical impedance spectroscopy of TiO_2 thin films air-annealed at 600 °C and exposed to air (empty squares) and to a range of ammonia concentrations (solid squares): (a) Nyquist plot and equivalent circuit; (b) imaginary impedance vs frequency plots. The arrow indicates the direction of increasing ammonia concentration. Experimental curve (squares), fitted curve (continuous line).

TABLE 2: Values of Equivalent Circuit Elements Used To Fit the EIS Data during Ammonia Adsorption on TiO_2 Thin Films Annealed at 600 °C and Relaxation Times and Sensitivity Values

	air	NH_3 1%	NH_3 4% 5 min	NH_3 4% 10 min	NH_3 4% 15 min
R_s (Ω)	77	69	68	69	67
R_1 (kΩ)	2.6	2.5	2.3	2.1	1.7
C_1 (nF)	0.88	0.87	0.87	0.87	0.89
τ_1 (μs)	2.3	2.2	2.0	1.8	1.5
S (%)		−4	−13	−20	−33

the increase in R_1 (circuit element in the order of kΩ) refers to the changes occurring because of modulation of the barrier height at the electrode/film junction or at any other relevant junction. Figure 3b shows a maximum in Z'' (complex impedance) which becomes larger and shifts to lower frequencies as the ammonia concentration increases resulting in larger relaxation times in the order of milliseconds (see Table 1).

EIS data during ammonia adsorption onto TiO_2 films annealed at 600 °C are shown in Figure 4 and are summarized in Table 2. Although the profile of the curves is similar to the ones presented in Figure 3, notice that as the ammonia concentration increases the impedance of the two-electrode cell decreases. The equivalent circuit used to fit the response of these films is similar to the one used to fit the responses in Figure 3 except for the fact that $n = 1$, converting the constant phase element Q into a perfect capacitor C. Figure 4b also shows a maximum in Z'', but it remains nearly constant in height and frequency upon exposure to ammonia in clear contrast with Figure 3b. The results in Table 2 show a decrease in R_1 as ammonia concentration increases and relaxation times are in the order of microseconds.

Several questions come to mind when comparing the values of Table 1 and Table 2. Films annealed at 600 °C have R_1 and C_1 sensibly lower than the values obtained from films annealed at 400 °C. The brickwork model used to interpret the EIS data

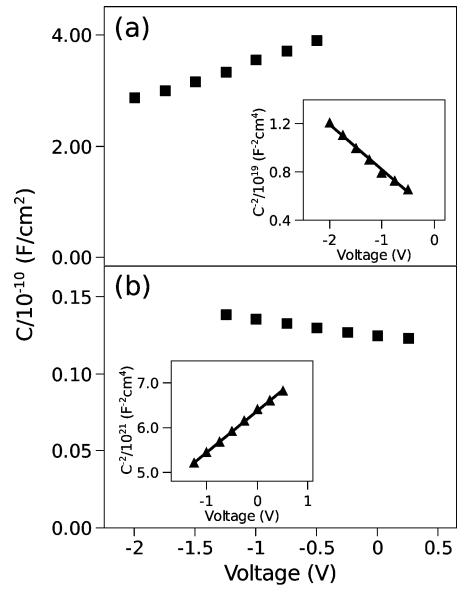

Figure 5. Capacitance versus potential curves of TiO_2 films annealed at (a) 400 °C and (b) 600 °C. Corresponding Mott−Schottky plots are shown as insets.

in metal oxide sensors[24] has a series of subcircuits made up by a resistor in parallel with a capacitor (i.e., Randles loop), which are related to the sensor response of grain bulks ($\sim 10^{-12}$ F), grain boundaries ($10^{-11}-10^{-8}$ F), and reaction at the film/electrode interface ($10^{-7}-10^{-5}$ F). Our observed range of capacitance values suggests a relevant role of grain boundaries.[25] Negatively charged oxygen ions are usually adsorbed at TiO_2 grain boundaries and can be removed by ammonia molecules resulting in a decrease of barrier height, an increase in capacitance, and a decrease in resistivity. This mechanism explains the behavior observed in films annealed at 600 °C but does not explain the increase in resistivity of films annealed at 400 °C. Given that XRD data does not show major changes in the crystal structure of the annealed films and that AFM images suggest a lower connectivity among the particles annealed at 400 °C (i.e., higher density of grain boundaries resulting in larger surface functionality), the differences in sensor response could be related to the abundance of hydroxyl groups or Ti^{3+} sites expected in films annealed at lower temperatures.

It is possible that at 400 °C the film is not completely oxidized giving a surface rich in low coordinated Ti atoms which will favor a charge transfer from the metal oxide to ammonia. Differences on the equivalent circuits describing the annealed films seem to agree with this hypothesis, since a nonideal capacitor is required for describing the sensor response of TiO_2 films annealed at 400 °C. Nonideality indicates a larger contribution of other physical and chemical processes such as film roughness, surface states, and diffusion of reactive chemical species. Moreover, the difference in relaxation times from milliseconds (TiO_2-400 °C) to microseconds (TiO_2-600 °C) suggests a more complex adsorption path in the 400 °C annealed film.

To further corroborate the anomalous response of TiO_2 films annealed at 400 °C, new samples were prepared and their capacitances were measured as a function of potential (Figure 5). For both annealing temperatures, the sample $C-V$ profiles indicate a weak dependence of the film capacitance on the potential applied (i.e., ill-defined electric fields or nearly flat band condition) which is characteristic of nanostructured films. Even so, there is a distinct change in slope for each annealing

temperature; for TiO_2-400 °C, the capacitance increases as the potential becomes more positive, while for TiO_2-600 °C, it decreases. Mott−Schottky (MS) plots[29] were included as insets in Figure 5 just to illustrate the changes observed. The negative slope of the MS plot in Figure 5a is characteristic of p-type junctions, while the positive slope in Figure 5b is characteristic of n-type materials. No attempt was made to obtain flat band potentials or doping levels from the MS model given its limited applicability in the absence of well-defined electric fields.

It is important to concede that in addition to changes in junction properties caused by annealing, the anomalous sensing behavior could also indicate a change in TiO_2 Fermi level (N-doping) caused by ammonia adsorption. However, to our knowledge, all reported N-doping by ammonia requires high temperature, potential bias, or aggressive chemical media,[26−28] which contrast with the mild conditions used during our adsorption experiments. More importantly, N-doped TiO_2 shows a decrease in band gap originated by the mixing of N (2p) states with O (2p) states but comparable photoelectrochemical/photocatalytic response with undoped TiO_2[26−28] (i.e., both are n-type materials that under illumination behave like photoanodes). It is interesting that we do not observe any anomalous sensing behavior in the resistor platform, which suggests that bulk properties are not involved and that instead the specific environment around the junctions is what is important.

Ab Initio Studies. To have a better understanding of the mechanisms responsible for the resistance variations observed in our TiO_2 samples, we present now ab initio pseudopotential DFT calculations addressing the NH_3 adsorption on small model Ti_xO_y ($x = 4$, $y = 6-8$) clusters. In Figure 6, we show first the lowest energy atomic arrays for a single NH_3 molecule adsorbed in various Ti_xO_y clusters with different sizes and chemical compositions. In this set of calculations, the atomic positions corresponding to the Ti_xO_y cluster will remain always fixed. From Figure 6a−d, we found that the ammonia species (1) is always attached in a molecular form, (2) adsorbs in an on-top configuration over a Ti atom of the structures, and (3) is characterized by having N−Ti bond lengths that vary in the range of 2.25−2.44 Å with the largest one being obtained for the structure shown in Figure 6d where the ammonia molecule is found to be coadsorbed with an hydroxyl group on the same Ti site. Actually, we obtain that the existence of different neighboring coadsorbed species strongly influences the orientation of the NH_3 molecule on the surface. In particular, OH groups are found to strongly attract the ammonia species. This is clearly seen when comparing the low-energy structures shown in Figure 6c and 6d where, in the former, the O_{oxy}−Ti−N angle (marked as beta in the figure) is equal to 91° while, in the latter, a close proximity between the coadsorbed species is found since an O_{hyd}−Ti−N angle of ∼74° is obtained. This is also the case when comparing Figure 6a and 6b where, in the latter, an appreciable reorientation of the ammonia molecule (defined by the alpha angle) toward the hydroxyl species is also found leading to the formation of a hydrogen bond (marked with a dashed line) between the two coadsorbed molecules (∼2.1 Å). In all cases [Figure 6a−d], the adsorption of the NH_3 group is characterized by an ammonia → Ti_xO_y direction for the charge transfer, and the amount of transferred charge strongly depends on the precise details of the local chemical and geometrical environment around the adsorption site. Clearly, this direction for the charge transfer is expected to decrease the resistance in materials showing n-type conductivity (electron-conducting systems) and is in line with our experimental data obtained in our synthesized TiO_2 films annealed at 600 °C.

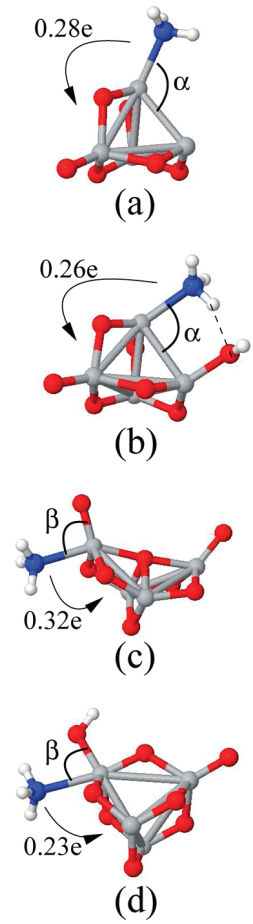

Figure 6. Lowest energy atomic arrays for a single NH_3 molecule adsorbed in various Ti_xO_y clusters ($x = 4$, $y = 6-8$) with different sizes and chemical composition. (a) $Ti_4O_6 + NH_3$, (b) $(Ti_4O_6)OH + NH_3$, (c) $Ti_4O_8 + NH_3$, and (d) $(Ti_4O_7)OH + NH_3$.

In Figure 7, we analyze the structure of some dissociated atomic configurations of NH_3 species adsorbed on our Ti_xO_y clusters by assuming a single dehydrogenation reaction. The low energy atomic configurations shown in Figure 7a−d were obtained from the optimized atomic structures shown in Figure 6a−d but in which a well-defined stripped H atom was allowed to be initially (1) adsorbed onto a neighboring Ti atom (in on-top [Figure 7a] and on-bridge configurations [Figure 7b]), (2) attached to a neighboring oxygen atom to form a OH group [Figure 7c], and (3) adsorbed on a neighboring OH group to try to induce the formation of a water molecule on the surface (Figure 7d). From Figure 7, we notice that in all cases, after the dehydrogenation reaction, the NH_2 fragments remain adsorbed in the Ti_xO_y clusters with considerably reduced N−Ti bond lengths that now vary in the range of 1.87−2.26 Å. With respect to the intermolecular interactions, we observe from Figure 7c that (in contrast to Figure 6d) less attractive interactions between an NH_2 group and the hydroxyl species are found since an O_{hyd}−Ti−N angle (marked as beta in the figure) of 90° is obtained.

With respect to the stripped H atom, we see from Figure 7a and 7b that it can be chemisorbed on a Ti site in both on-top and on-bridge configurations with H−Ti bond lengths of 1.74 Å in Figure 7a as well as of 1.81 and 1.74 Å in Figure 7b. Most interestingly, we notice from Figure 7d that when a N−H bond breaks and the dissociated hydrogen adsorbs on a neighboring OH group, the formation of a water molecule is obtained which is found to be unstable and which desorbs from

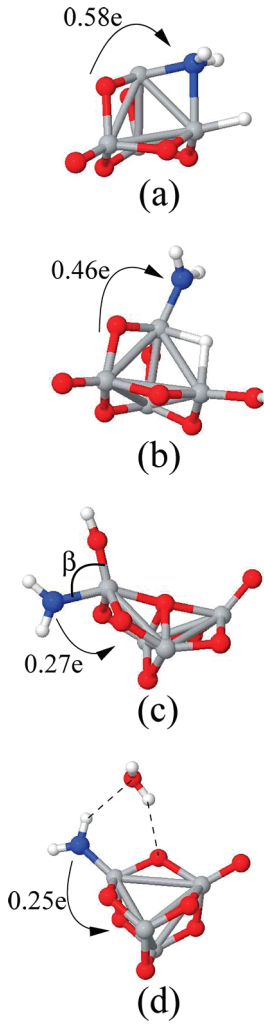

Figure 7. Low energy atomic configurations of some dissociated atomic configurations of NH_3 species adsorbed on the various Ti_xO_y ($x = 4$, $y = 6-8$) clusters shown in Figure 6 assuming a single dehydrogenation reaction. (a) $Ti_4O_6 + (NH_2 + H)$, (b) $(Ti_4O_6)OH + (NH_2 + H)$, (c) $(Ti_4O_7)OH + (NH_2)$, and (d) $Ti_4O_7 + (NH_2 + H_2O)$.

the surface of the Ti_xO_y cluster. However, we see that after being detached from the structure, it remains trapped near the remaining NH_2 group in a physisorbed state by means of well-defined O−H bonds (marked with dashed lines) having lengths of 2.35 and 2.18 Å.

In Figure 7, some of the low energy dissociated atomic configurations are characterized by having a reverse $Ti_xO_y \rightarrow (NH_2 + H)$ direction for the charge transfer. This is the case of the configurations shown in Figure 7a and 7b where, in contrast with our previous results, 0.58 and 0.46 electrons are transferred, respectively, from the Ti_xO_y clusters to the chemisorbed NH_2 and H species. Clearly, this direction for the charge transfer, which occurs when the dissociation of the ammonia molecule is present on the surface, will increase the resistivity of materials characterized by n-type conductivity as is the case in our measurements performed on TiO_2 samples annealed at 400 °C. In contrast, H stripping and subsequent adsorption on neighboring oxygen or hydroxyl groups, as shown in Figure 7c and 7d, lead to the expected adsorbate → Ti_xO_y behavior in which ∼0.26 electrons are transferred in both cases, which is in good agreement with our theoretical data shown in Figure 6.

Concerning the relative stability between the molecular and dissociated atomic arrays shown in Figures 6 and 7, the

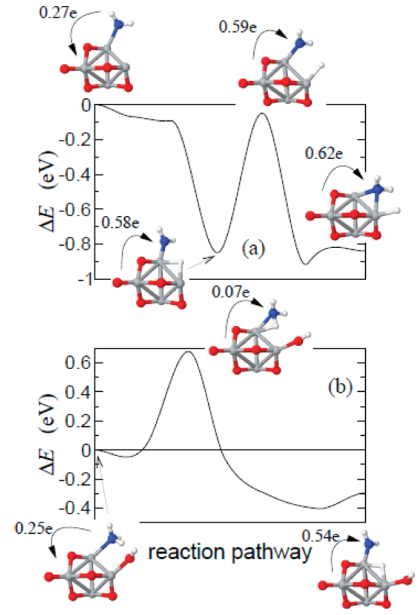

Figure 8. Reaction energy paths connecting the locally stable atomic configurations of Figure 6 (a, b) with Figure 7 (a, b) and assuming fully relaxed precursor and final atomic configurations.

dehydrogenated configuration of Figure 7a is more stable than the molecularly adsorbed phase shown in Figure 6a by ∼0.6 eV. Second, Figures 6b and 7b are found to be very close in energy although the dissociated structure is found to be less stable by 0.1 eV. Finally, when comparing Figures 6c and 7c, as well as Figures 6d and 7d, we find that the dissociated configurations are less stable by 0.4 and 0.8 eV, respectively. We expect, thus, that the ammonia molecule will be in its dehydrogenated state (see Figure 7a) on the surface of Ti_xO_y clusters with poorly coordinated Ti sites, a local atomic environment that could be present in our samples annealed at 400 °C and that has been characterized by an anomalous behavior for the charge transfer between the adsorbed species and the cluster structures.

After the determination of several low energy atomic configurations in both molecular (Figure 6) and dissociated (Figure 7) states, we calculated the reaction paths as well as the energy barriers which link the locally stable atomic configurations shown in the previous figures. In general, the results of fixed and fully relaxed systems (shown in the Supplementary Information and in Figure 8, respectively) indicate that the paths which describe the dehydrogenation reaction onto neighboring Ti sites possess lower reaction barriers when compared to those in which hydroxyl or water formation occurs in the surface of our considered structures. We found that well-defined geometrical and chemical details of the titanium dioxide structures will promote or hinder the dissociation of ammonia species by substantially changing the activation barriers, and interestingly, in the cases where the reverse $Ti_xO_y \rightarrow (NH_2 + H)$ direction for the charge transfer is obtained, we notice (as seen in Figure 8) that it occurs as soon as the stripped H atom is bonded to the underlying Ti atom.

Since notable atomic relaxations in our Ti_xO_y cluster structures are expected to occur upon ammonia adsorption, Figure 8 shows the results of calculations in which we fully relaxed all the atoms of our $Ti_xO_y + NH_3$ systems. As representative examples, Figure 8 (a, b) shows the reaction energy paths linking Figure 6 (a, b) with Figure 7 (a, b), respectively, but now including fully relaxed precursors and final atomic configurations. In Figure 8a, the

most important feature is the relatively small energy barrier that was found in our unrelaxed calculation (~0.35 eV, see Figure 1 of the Supporting Information) as it is now completely removed by the reconstruction of the cluster atoms. Consequently, once the NH_3 molecule is chemisorbed on the surface of the cluster, it will move spontaneously (with no barrier) to the atomic configuration in which the stripped hydrogen atom is attached in an on-bridge configuration (see the inset of Figure 8a) and for which a reverse $Ti_xO_y \rightarrow (NH_2 + H)$ direction for the charge transfer (~0.58e) is also obtained. Finally, from Figure 8b, we found that, after the full relaxation of the system, the reaction energy path is still characterized by a single-step process and that the height of the energy barrier is almost the same as the unrelaxed system at about 0.7 eV. Interestingly, in this case, and in contrast to the relative stability obtained from Figures 6b and 7b, we notice that the final dehydrogenated configuration has become now clearly the most stable adsorbed phase (by ~0.35 eV) confirming the here-reported trend in which ammonia molecules prefer to be dissociated in the presence of poorly coordinated Ti sites around the adsorption site. This finding is also in agreement with the reports of N-doped titania,[26] where XPS data confirms that all incorporated nitrogen is substitutional on the oxygen site (i.e., nitrogen is filling oxygen vacancies in poorly coordinated Ti-sites).

Conclusion

Thin films of TiO_2 were elaborated by dip-coating process in sol−gel solutions, were annealed in air at 400 and 600 °C, and were used as ammonia Schottky sensors monitored by electrochemical impedance spectroscopy. In contrast to the sensing behavior of films annealed at 600 °C, an anomalous increase in resistance and capacitance was observed in TiO_2 films annealed at 400 °C and could be related to the abundance of hydroxyl groups or Ti^{3+} sites expected in films annealed at lower temperatures. Our ab initio studies showed that the precise geometrical and chemical details of the local atomic environment around the adsorption site determine the magnitude and direction of the charge transfer as well as the nondissociation or dissociation of NH_3 species on the oxide surface. We demonstrated that the energy barriers that need to be overcome to achieve a single dehydrogenation of the NH_3 species are considerably reduced when the reaction takes place on poorly coordinated Ti sites located around the adsorption site. As a consequence, the differences in equivalent circuits and relaxation times can be attributed to the different structure and chemical composition of the TiO_2 surface induced by the different thermal treatments.

Acknowledgment. Financial support from DGAPA-UNAM (IN104309), PUNTA-UNAM, CONACYT-México (49100, 45982, and 50650), and PROMEP-México are gratefully acknowledged as well as the fellowship (M. Sánchez) provided by CONACYT-México. We thank M. Miranda, R. Morán, and M. L. Román for technical assistance and XRD analyses.

Supporting Information Available: Details of the reaction energy paths of unrelaxed systems (i.e., keeping the atomic position of Ti_xO_y clusters fixed) is available free of charge via the Internet at http://pubs.acs.org.

References and Notes

(1) Skubal, L. R.; Meshkov, N. K.; Vogt, M. C. *J. Photochem. Photobiol., A* **2002**, *148*, 103.
(2) Taurino, A. M.; Capone, S.; Boschetti, A.; Toccoli, T.; Verucchi, R.; Pallaoro, A.; Siciliano, P.; Iannota, S. *Sens. Actuators, B* **2004**, *100*, 177.
(3) Savage, N. O.; Akbar, S. A.; Dutta, P. K. *Sens. Actuators, B* **2001**, *72*, 239.
(4) Devi, G. S.; Hyodo, T.; Shimizu, Y.; Egashira, M. *Sens. Actuators, B* **2002**, *87*, 122.
(5) Varghese, O. K.; Gong, D.; Paulose, M.; Ong, K. G.; Grimes, C. A. *Sens. Actuators, B* **2003**, *93*, 338.
(6) Mor, G. K.; Carvalho, M. A.; Varghese, O. K.; Pishko, M. V.; Grimes, C. A. *J. Mater. Res.* **2004**, *19*, 628.
(7) Ruiz, A.; Arbiol, J.; Cirera, A.; Cornet, A.; Morante, J. R. *Mater. Sci. Eng., C* **2002**, *19*, 105.
(8) Ruiz, A. M.; Sakai, G.; Cornet, A.; Shimanoe, K.; Morante, J. R.; Yamazoe, N. *Sens. Actuators, B* **2003**, *93*, 509.
(9) Ruiz, A.; Cornet, A.; Morante, J. R. *Thin Solid Films* **2004**, *100*, 256.
(10) Islam, M. R.; Kumazawa, N.; Takeuchi, M. *Appl. Surf. Sci.* **1999**, *142*, 262.
(11) Sánchez, M.; Guirado-López, R. A.; Rincón, M. E. *J. Mater. Sci.: Mater. Electron.* **2007**, *18*, 1131.
(12) Guirado-López, R. A.; Sánchez, M.; Rincón, M. E. *J. Phys. Chem. C* **2007**, *111*, 57.
(13) Yamada, T. *Appl. Phys. Lett.* **2006**, *88*, 83106.
(14) Yu, M.-J.; Yang, D.-H.; Lee, S.-W.; Kunitake, T.; Hayashi, K.; Toyo, K. *Sens. Actuators, B* **2007**, *123*, 259.
(15) Salgado, J. R.; Djurado, E.; Fabry, P. *J. Eur. Ceram. Soc.* **2004**, *24*, 2477.
(16) Carrara, S.; Bavastrello, V.; Ricci, D.; Stura, E.; Nicolini, C. *Sens. Actuators, B* **2005**, *109*, 221.
(17) Henkelman, G.; Uberuaga, B. P.; Jónsson, H. *J. Chem. Phys.* **2000**, *113*, 9901.
(18) Lowdin, P. O. *J. Chem. Phys.* **1950**, *18*, 365.
(19) Cullity, B. D. *Elements of X-ray Diffraction;* Addison-Wesley Publishing Company Inc: Reading, MA, 1978; p 262.
(20) Baroni, S.; Dal Corso, A.; de Gironcoli, S.; *Quantum Espresso*, 2007; http://www.pwscf.org/.
(21) Perdew, J. P.; Wang, Y. *Phys. Rev. B* **1992**, *45*, 13249.
(22) Lai, W.; Hailew, S. M. *J. Am. Ceram. Soc.* **2005**, *88*, 2979.
(23) Orazem, M. E.; Shukla, P.; Membrino, M. A. *Electrochim. Acta* **2002**, *47*, 2027.
(24) Ruíz-Morales, J. C.; Marrero-López, D.; Irvine, J. T. S.; Nuñez, P. *Mater. Res. Bull.* **2004**, *39*, 1299.
(25) Wierzbicka, M.; Pasierb, P.; Rekas, M. *Physica B* **2007**, *387*, 302.
(26) Mor, G. K.; Varghese, O. K.; Paulose, M.; Shankar, K.; Grimes, C. A. *Sol. Energy Mater. Sol. Cells* **2006**, *90*, 2011.
(27) Vitiello, R. P.; Macak, J. M.; Ghicov, A.; Tsuchiya, H.; Dick, L. F. P.; Schmuki, P. *Electrochem. Commun.* **2006**, *8*, 544.
(28) Han, F.; Kambala, V. S. R.; Srinivasan, M.; Rajarathnam, D.; Naidu, R. *Appl. Catal., A* **2009**, *359*, 25.
(29) Orazem, M. E.; Tribollet, B. *Electrochemical Impedance Spectroscopy*; John Wiley & Sons Inc.: Hoboken, NJ, 2008; p 228.

JP9024014